Biogeosciences Discuss., 12, 13631–13673, 2015
www.biogeosciences-discuss.net/12/13631/2015/
doi:10.5194/bgd-12-13631-2015

Biogeosciences Discussions
Open Access

Spring bloom onset in the Nordic Seas

A. Mignot[1], **R. Ferrari**[1], **and K. A. Mork**[2,3]

[1]Massachusetts Institute of Technology, Cambridge, MA, USA
[2]Institute of Marine Research, Bergen, Norway
[3]Bjerknes Centre for Climate Research, Bergen, Norway

Received: 31 July 2015 – Accepted: 7 August 2015 – Published: 21 August 2015

Correspondence to: A. Mignot (mignot@mit.edu)

Published by Copernicus Publications on behalf of the European Geosciences Union.

Abstract

The North Atlantic spring bloom is a massive annual growth event of marine phytoplankton, tiny free-floating algae that form the base of the ocean's food web and generates a large fraction of the global primary production of organic matter. The conditions that trigger the onset of the spring bloom in the Nordic Seas, at the northern edge of the North Atlantic, are studied using in-situ data from five bio-optical floats released above the Arctic Circle. It is often assumed that spring blooms start as soon as phytoplankton cells daily irradiance is sufficiently abundant that division rates exceed losses. The bio-optical float data instead suggest the tantalizing hypothesis that Nordic Seas blooms start when the photoperiod, the number of daily light hours experienced by phytoplankton, exceeds a critical value, independently of division rates. This bloom behavior may be explained by realizing that photosynthesis is impossible during polar nights and phytoplankton enters in a dormant stage in winter, only to be awaken by a photoperiodic trigger. While the first accumulation of biomass recorded by the bio-optical floats is consistent with the photoperiod hypothesis, it is possible that some biomass accumulation started before the critical photoperiod but at levels too low to be detected by the fluorometers. Thus more precise observations are needed to test the photoperiod hypothesis.

1 Introduction

The Nordic Seas (Norwegian, Greenland, and Iceland Seas) experience some of the largest carbon dioxide (CO_2) fluxes anywhere in the ocean resulting in a carbon uptake of 20–85 g C m^{-2} yr^{-1} (Takahashi et al., 2002). In the Greenland Sea it has been estimated that one third of the annual carbon uptake is driven by export production from biological activity, while the rest is the result of CO_2 dissolution in cold waters that sink into the abyss (Skjelvan et al., 2005). Most of the biological production occurs during ephemeral spring blooms lasting only a few weeks. A good understanding of the condi-

BGD
12, 13631–13673, 2015

tions that trigger these blooms is thus a prerequisite to quantify and model the carbon budget of the Nordic Seas.

In winter, phytoplankton populations decay because losses from respiration, grazing, and viral infections exceed growth. Blooms develop in spring when division rates increase and/or loss rates decrease. Phytoplankton division rates increase with abundance of nutrients and light. At high latitudes nutrients are plentiful in winter, because the strong upper ocean mixing generated by winds and cooling brings deep nutrients to the surface. Thus light appears to be the limiting factor for winter growth in the sub-polar gyres, as argued in the seminal works of Gran and Braarud (1935), Riley (1946) and Sverdrup (1953). However, it was soon noted that the surface light levels are sufficient for photosynthesis growth even at these latitudes. Thus the light limitation has been attributed to mixing that keeps phytoplankton cells away from the well-lit surface for long periods of time. Sverdrup (1953) formalized this view and suggested that blooms develop when mixing weakens at the end of winter and phytoplankton spend more time close to the surface to receive enough light to grow in spite of losses. More recently, Behrenfeld (2010) pointed out that blooms can also develop when grazing decreases in winter. Mixing dilutes both phytoplankton and herbivores reducing their encounter rate and hence the grazing rates. If mixing is strong enough to substantially reduce the losses due to grazing, but not too strong to limit light exposure and growth, a bloom can therefore develop.

These ideas dominate thinking about bloom dynamics, but they may not be as relevant to understand blooms in the Nordic Seas. At these extreme latitudes, insolation drops dramatically in winter. North of the Arctic Circle, no light is received at the ocean surface during the polar nights. Phytoplankton growth is simply impossible for days to weeks, depending on the latitude, regardless of mixing levels. It is therefore natural to ask how do phytoplankton populations survive such harsh conditions and what triggers their resurgence in spring.

In this manuscript, we study the development of blooms in the Nordic Seas using in-situ profiles of phytoplankton from five bio-optical floats released north of the Arc-

BGD
12, 13631–13673, 2015

tic Circle. The floats were instrumented with miniaturized bio-optical sensors, which measure chlorophyll concentrations in the upper kilometer of the ocean for one to two years. The data suggest that at these high latitudes, one of two possible scenarios may explain the onset of the Nordic Seas blooms observed by the floats: the critical depth hypothesis or the critical photoperiod hypothesis.

The paper is organized as follows. We introduce the datasets used in the study in Sect. 2. Section 3 provides a preliminary analysis of the data with the conclusion that two possible interpretations can explain the onset of the Nordic Seas blooms. In Sect. 4, we develop the theoretical framework to test the two hypotheses. This framework is then used in Sect. 5. Finally, Sect. 6 summarizes and discusses the results.

2 Data

2.1 Floats deployed north of the Arctic Circle

Our results are based on measurements collected with five bio-optical profiling floats deployed in the Nordic Seas, North of the Arctic Circle, by the Institute of Marine Research in Norway (see Fig. 1 and Table 1). Three floats were deployed in 2010 (IMR1, IMR2, IMR3) and two additional floats were deployed in November 2013 and January 2014 respectively (IMR4, IMR6). The IMR1, IMR2, IMR3, IMR4 and IMR6 float data were downloaded from the Coriolis data center (http://www.coriolis.eu.org/). The IMR4 float data were downloaded from the OAO website (http://www.oao.obs-vlfr.fr/). The three floats deployed in 2010 were in the water for two years and returned observations of six spring blooms. The floats deployed in 2013–2014 are still operating and sampled the 2014 spring bloom.

We consider measurements made by the floats IMR1, IMR2 and IMR3 from September 2010 to June 2011 and from September 2011 to June 2012, time periods long enough to capture the onset of the spring blooms – the float IMR3 was deployed in November 2010 and hence the analysis start in November. Measurements from

BGD
12, 13631–13673, 2015

floats IMR4 and IMR6 span the interval from their deployment date (January 2014 and November 2013, respectively) to June 2014.

2.2 Float deployed South of the Arctic Circle

One bio-optical float (IMR5) was deployed south of the Arctic Circle in January 2014 and did not experience a polar night. This float is used to compare blooms north and south of Arctic Circle and better illustrate the effect of complete darkness on the phytoplankton dynamics. The IMR5 float data were downloaded from the Coriolis data center (http://www.coriolis.eu.org/).

2.3 Floats instrumentation and calibration

The IMR1, IMR2, IMR3, IMR5 and IMR6 floats were APEX float profilers, equipped with a WET Labs ECO FLNTU comprising a chlorophyll fluorometer, and a backscattering sensor at 700 nm. The IMR1-3 and IMR5 floats included a SEABIRD dissolved oxygen sensor while IMR6 float included an Aanderaa optode [O_2] sensor. The IMR4 float was a PROVOR profiler equipped with a Satlantic OC4 radiometer measuring downwelling irradiance at 380, 412, and 490 nm and Photosynthetically Available Radiation (PAR) integrated between 400 and 700 nm, a WET Labs ECO triplet comprising a chlorophyll fluorometer, a backscattering sensor at two wavelengths (532 and 700 nm) and an Aanderaa optode [O_2] sensor.

The IMR1, IMR2, IMR3, IMR5 and IMR6 floats nominal mission included CTD and optical profiles from 1000 m to the surface. The sampling resolution was 25 m from 1000 to 350 m, 10 m from 350 to 100 m, and 5 m from 100 to the surface. The upward casts were repeated every 5 or 10 days. The floats typically emerged from the sea around midnight, but, occasionally, they reached the surface in the morning or in the afternoon.

BGD
12, 13631–13673, 2015

The IMR4 float nominal mission included CTD and bio-optical profiles from 1000 m to the surface. The optical and CTD sampling resolution was one meter. The upward casts were repeated every 5 days. The floats emerged from the sea around local noon.

The CTD data were quality-controlled using the standard Argo protocol (Wong et al., 2010). The fluorescence raw signals (counts) were transformed into Chl *a* concentration, [Chl *a*], expressed in mg m^{-3} via a scale factor and after the nominal instrument-specific dark counts have been subtracted. The manufacturer provides two parameters for converting measured fluorescence counts to estimated [Chl *a*]: a nominal instrument-specific dark counts and a scale factor expressed in mg m^{-3} relating measured fluorescence minus the dark counts to [Chl *a*]. We tested the accuracy of the scale factor provided by the manufacturer again a slope determined by a regression between the float fluorescence in the upper 40 m (minus the dark count) and [Chl *a*] estimates from Moderate Resolution Imaging Spectroradiometer (MODIS); following the method proposed by Boss et al. (2008). We used the 8-day level 3 MODIS composites in $0.2^{\circ} \times 0.2^{\circ}$ boxes centered on the float locations for match up data. We did not have enough match-up data for floats IMR5 and IMR6 (i.e., < 10), so we did not perform the comparison for these two floats. We found that the manufacturer's scale factors for our fluorometers (IMR1:0.0072 mg m^{-3} $count^{-1}$, IMR2: 0.0074 mg m^{-3} $count^{-1}$ IMR3: 0.0074 mg m^{-3} $count^{-1}$ IMR4: 0.0097 mg m^{-3} $count^{-1}$) were always higher than the slope estimated by the regression with satellite products [IMR1:0.0051 mg m^{-3} $count^{-1}$, 59 match-ups, correlation coefficient $R = 0.62$; IMR2: 0.0051 mg m^{-3} $count^{-1}$, 54 match-ups, $R = 0.81$; IMR3: 0.0031 mg m^{-3} $count^{-1}$, 50 match-ups, $R = 0.84$; IMR4: 0.0021 mg m^{-3} $count^{-1}$, 32 match-ups, $R = 0.43$). As proposed by Boss et al. (2008), we used the MODIS slope to calibrate the fluorescence into [Chl *a*]. For floats IMR5 and IMR6, we used the scale factor provided by the manufacturer (IMR5: 0.0073 mg m^{-3} $count^{-1}$, IMR6: 0.0073 mg m^{-3} $count^{-1}$).

BGD
12, 13631–13673, 2015

2.4 Float estimates of mixed layer and euphotic layer depth

In the analysis to follow, we will need estimates of the mixed layer depth, the layer where density is well homogenized, and the euphotic layer depth, the depth where the downwelling irradiance is reduced to 1 % of its surface value.

For all floats but one, the mixed layer depth (H) was computed as the depth at which the density change from its value at 10 m is $\Delta\sigma_\theta = 0.005\,\mathrm{kg\,m^{-3}}$ (Kara et al., 2000, 2003). We chose the value of $\Delta\sigma_\theta$ that best tracked the region of weak stratification in our dataset. This value is consistent with the study of Brainerd and Gregg (1995) who also found that a $\Delta\sigma_\theta$ of 0.0025–0.005 $\mathrm{kg\,m^{-3}}$ often marks the base of the active turbulent surface layer. The salinity sensor was defective in the float IMR2 and thus H was computed as the depth at which the temperature change from its value at 10 m is $\Delta\theta = 0.1\,^\circ\mathrm{C}$, which corresponds to $\Delta\sigma_\theta$ 0.005 $\mathrm{kg\,m^{-3}}$ for a salinity of 35.2 representative of values observed in the Nordic Seas.

The surface value of [Chl *a*] ($[\mathrm{Chl}]_{\mathrm{ML}}$, $\mathrm{mg\,m^{-3}}$) was calculated as the average within the mixed layer (ML). The vertical integral of [Chl *a*] ($<\mathrm{Chl}>$, $\mathrm{mg\,m^{-2}}$) was obtained by integrating the vertical profile of [Chl *a*] from the surface down to the ML base. The euphotic layer depth (Z_{eu}), defined as the depth at which the light intensity is 1 % of its surface value, was calculated from $[\mathrm{Chl}]_{\mathrm{ML}}$ using the empirical relationship derived by Morel et al. (2007) from a global datasets of ship-based measurements of Z_{eu} and surface [Chl *a*] :

$$\log_{10}Z_{\mathrm{eu}} = 1.524 - 0.436 \times \log_{10}[\mathrm{Chl}]_{\mathrm{ML}} - 0.0145 \times (\log_{10}[\mathrm{Chl}]_{\mathrm{ML}})^2 + 0.0186 \times (\log_{10}[\mathrm{Chl}]_{\mathrm{ML}})^3 \quad (1)$$

2.5 Atmospheric and solar variables

In our analysis, we will additionally need estimates of the heat and freshwater fluxes that drive upper ocean turbulence and the photosynthetically active radiation (PAR). The hourly net atmospheric heat fluxes (Q_0 in $\mathrm{W\,m^{-2}}$) were taken from the ECMWF

BGD
12, 13631–13673, 2015

ERA-interim reanalysis (Dee et al., 2011). We ignored the freshwater fluxes that are a minor contributor to upper ocean turbulence in the winter North Atlantic (Ferrari et al., 2014). Time series of the heat fluxes along the float trajectories were then generated by averaging the daily ERA-interim values in one by one degree bins around the float daily positions.

The clear sky instantaneous PAR in mol photons $m^{-2}\,s^{-1}$, $iPAR(0,t)_{clear}$, was calculated using the Gregg and Carder solar irradiance model for a free-cloud sky (Gregg and Carder, 1990). The reduction of the photosynthetically active radiation due to clouds was estimated with the formulation of Antoine and Morel (1996):

$$iPAR(0,t) = iPAR(0,t)_{clear}[1 - 0.75 \times \Delta/(1 - 0.115)], \quad (2)$$

with

$$\Delta = 0.632 \times c - 0.0019\alpha, \quad (3)$$

where c is the total cloud cover, and α is the solar elevation at noon (in degrees). The total cloud cover c, varying from 1 for an overcast sky to 0 for a clear sky, was taken from ECMWF ERA-interim reanalysis averaged along the float trajectories as described for the heat fluxes.

Finally, in some calculations we will need information about the length of daytime. The length of daytime (dl, hours) was estimated with the package geosphere from the R software (R Development Core Team, n.d.), which computes the length of the daytime for a flat surface for a given latitude and day of year (Forsythe et al., 1995).

3 Data analysis

From fall to spring, in each of the eight years sampled by the floats north of the Arctic Circle (two years each from IMR1, IMR2, IMR3 and one year from IMR4 and IMR6), we observed the same pattern in Chl *a* concentration. Figure 2 shows the potential

BGD
12, 13631–13673, 2015

density anomaly (σ_θ), and [Chl *a*], acquired by the float IMR2 from September 2011 to June 2012. (Equivalent figures for the other seven years are displayed in the Supplement Figs. S1–S8.) The ML and euphotic depths are marked as continuous and dashed black lines respectively. Figure 2a shows that in fall, from September to December, the [Chl *a*] decreased and the ML deepened. The fluorescence signal dropped to its minimum value from late December-early January during the polar night and the values were essentially uniform from the ML down to 1000 m (not shown) for the following several weeks. We are lead to suspect that the profiles were uniform, because the [Chl *a*] dropped too low to be detected by the fluorometer, a hypothesis further supported by the backscattering profiles which were also low and uniform over the same depth range.

To test whether the polar night ML [Chl *a*] was too low to be detected by the fluorometer, we compared the fluorescence measurements collected in the ML, where one expects to find some low [Chl *a*], with those deeper than 900 m, where no [Chl *a*] is expected and the fluorescence values can be used as an estimate of the dark signal, i.e. fluorescence values measured in the absence of [Chl *a*]. For each profile collected from December to April, we checked whether the distribution of fluorescence values in the ML was significantly different from the distribution of values below 900 m using a two-sample Kolmogorov-Smirnov test. The *K*-*S* test confirmed that during winter, the ML fluorescence values were not different from the deep values at the 99 % confidence interval (marked with an asterisk in the figures). In other words, the winter [Chl *a*] in the ML was too low to be detected by the fluorometer.

The winter [Chl *a*] profiles from float IMR5, which profiled south of Arctic Circle in winter, were very different from those north of the Arctic Circle as shown in Fig. S9. These profiles were characterized by significantly higher fluorescence values in the ML than at deeper depths, most likely because the [Chl *a*] remained high enough to be detected by the fluorometer. This last point is important, because it suggests that a period of complete darkness depletes the phytoplankton biomass so dramatically that traditional fluorometers cannot detect its concentration.

BGD
12, 13631–13673, 2015

The ML fluorescence values north of the Arctic Circle emerged from the fluorometer noise level after the end of the polar night. The time of "emergence from noise" t_E, was defined as the time (second white vertical line in Fig. 2), when the ML fluorescence values became significantly greater than the deep fluorescence values as per the *K-S* test. The positions of the floats at t_E for all floats deployed north of the Arctic Circle are shown as a black dots in Fig. 1.

The net accumulation of chlorophyll starting at t_E was detected both in surface $[Chl]_{ML}$ and vertically integrated $< Chl >$, and lasted until June–July. However, we cannot say whether accumulation started at t_E or earlier when the fluorescence values were too low to be detected by the fluorometer. Given that photoautotrophic growth is not possible without light, we can conclude that the bloom must have started sometime between the end of the polar night and t_E. We will refer to this time interval as Δt_{onset} (shown as a gray shading area in Fig. 2).

As a first step to assess what triggered the bloom onset, we investigated whether there were some consistent changes in the physical environment favorable to bloom onset during Δt_{onset} in all the eight years sampled by the floats north of the Arctic Circle. Figure 3a and b show the surface heat fluxes and the ML depth with time shifted so that the origin is at $t = t_E$ for each of the eight float years. During the weeks preceding t_E, the surface heat flux remained negative for six out of the eight years, suggesting that mixing was active. For those six years, the ML depth was sometimes shoaling and sometimes deepening, ranging between 50 m and 300 m. Since the bloom started at or before t_E, it appears that in these six cases the bloom was not triggered by a subsidence in mixing as in Taylor and Ferrari's (2011) hypothesis or by a shoaling of the ML as predicted by Sverdrup (1953). However, the increase in [Chl *a*] and thus, possibly, the bloom onset, coincided with the shutdown of convection and the sudden shoaling of the ML for floats IMR2 and IMR3, consistent with both Taylor and Ferrari's and Sverdrup's hypotheses. These two float years differed from the other six in that the MLs were very deep, in excess of 600 m, before the bloom onset.

BGD
12, 13631–13673, 2015

Figure 3c shows that the solar radiation reaching the surface increased monotonically by close to two orders of magnitude during the weeks preceding $t = t_E$, suggesting that increase in PAR played an important role in all bloom onsets. Figure 3d further shows that at $t = t_E$, the time when the accumulation of phytoplankton biomass was first detected by the fluorometer, the daylength was between 9 and 11 h for the six float years that clearly did not bloom in response to changes in heat fluxes and ML depth.

Two possible bloom onset scenarios emerge from this simple preliminary analysis of the float data. One interpretation is that all bloom onsets are consistent with the critical depth hypothesis. In six cases, the bloom started because phytoplankton division rate increased rapidly as the surface insolation increased, and became larger than the phytoplankton loss rates (notice that these events are not quite consistent with Sverdrup's assumption that it is changes in the ML depth rather than changes in surface insolation that are key). In the remaining two cases, it appears that the ML was so deep that the increase in surface insolation was not sufficient to drive phytoplankton division rates larger than the loss rates until the ML shoaled. However, it is also possible that the bloom started before the ML shoaling, but the biomass accumulation was so weak as to go undetected by the fluorometers.

A second interpretation is that blooms started at $t = t_E$, when the accumulation of phytoplankton biomass was first detected by the fluorometer, and the photoperiod (the duration of a phytoplankton cell daily exposure to light) reached a critical value of 10 ± 1 h. For the six events with shallow MLs, the photoperiod was equal to the daylength (see Fig. 4). In the two cases with deep MLs, the phytoplankton did not experience 10 ± 1 h of light until the mixing subsided and allowed cells to linger at the surface. In the next section, we develop the theoretical framework to test these two possible scenarios.

BGD
12, 13631–13673, 2015

4 Theory

4.1 Critical depth hypothesis

Following Sverdrup (1953), the changes in phytoplankton concentration $P(z,t)$ in response to changes in light, grazing and vertical mixing can be described by a partial differential equation:

$$\frac{\partial P(z,t)}{\partial t} = \mu(z,t)P(z,t) - m(z,t)P(z,t) + \frac{\partial}{\partial z}\left(\kappa_T(z,t)\frac{\partial P(z,t)}{\partial z}\right), \quad (4)$$

where z is the vertical coordinate, t is time, μ is the cell division rate, m is the phytoplankton loss rate and κ_T is the vertical eddy diffusivity, which represents the rate at which turbulence mixes phytoplankton in the vertical. The effect of light on growth is captured by the depth and time dependence of the division rate. Nutrient limitation on growth is ignored, because in the early phase of blooms in the Nordic Seas nutrients are plentiful. The depth and time dependence of the loss rate represents the variations in respiration and grazing. Finally, we ignore the effect of lateral advection of phytoplankton by oceanic currents. This is a reasonable assumption as long as the currents are weak or the phytoplankton concentrations are uniform in the horizontal. We cannot test whether this is always the case for the float data, so we will use this equation as a working hypothesis and check to what extent the terms included in the right hand side are sufficient to explain the observed changes in $P(z,t)$.

When turbulence is strong, like in the Nordic Seas winter, the phytoplankton is mixed so fast that it remains uniform within the ML and we can ignore the z dependence in P. Integrating Eq. (4) over the mixed layer and assuming that there is no phytoplankton flux through the surface and the ML base, we obtain an expression for the phytoplankton growth rate,

$$\int_{-H}^{0} \frac{\partial P}{\partial t} \mathrm{d}z = \langle\mu\rangle P - \langle m\rangle P, \quad (5)$$

BGD
12, 13631–13673, 2015

where ⟨⟩ represents the vertical integral between the surface and the ML base at $z = -H$. The total population size can grow when the left-hand size is positive, or

$$\langle \mu \rangle \geq \langle m \rangle. \tag{6}$$

If following Sverdrup (1953), we further assume that the losses are independent of depth, since they depend on phytoplankton and zooplankton concentrations which are uniform with depth, then $\langle m \rangle = Hm$, and accumulation occurs if the mixed layer depth is shallower than a critical depth

$$H \leq H_c = \frac{\langle \mu \rangle}{m}, \tag{7}$$

or state differently; when the daily mixed layer averaged division rate is greater than the loss rates:

$$\frac{1}{H}\langle \mu \rangle \geq m. \tag{8}$$

Despite its simplicity, the condition necessary for bloom onset in the limit of strong turbulence is difficult to test quantitatively with profiling float data. Testing Eq. (8) requires in situ observations of phytoplankton division and loss rates, which presently cannot be measured with autonomous platforms. Phytoplankton division rate can however be estimated using bio-optical models. Then, phytoplankton loss rates can then be derived from Eq. (5) by subtracting the net accumulation rate (i.e., $\frac{1}{P}\int_{-H}^{0} \frac{\partial P}{\partial t} \mathrm{d}z$ from $\langle \mu \rangle$).

To avoid the confusion down the road, it is worth emphasizing that the critical depth framework remains the key approach to study the development of blooms. There is however, an ongoing discussion as to what process drives Eq. (7) to be first satisfied at bloom onset. Sverdrup (1953) hypothesized that Eq. (7) is typically satisfied at the end of winter when the ML shoals. Behrenfeld (2010) argued that Eq. (7) can be satisfied already in late fall if m decreases faster than $\frac{1}{H}\langle \mu \rangle$ when the ML deepens. It is also possible for blooms to start in response to an increase in light, hence μ, with no changes in the other variables. In the following, we will use the critical depth framework to interpret the float data, with the goal of determining what process first trigger the bloom.

BGD
12, 13631–13673, 2015

4.1.1 Phytoplankton division rates

The division rate μ in Eq. (4) represents the division rate of the overall phytoplankton population. Thus, its quantification would require detailed information of the species present in the water column. Unfortunately, species information is very hard to collect. The only study that reported data about the species abundance in open-ocean Nordic Seas during the time of bloom onset dates back Halldal (1953). The study tracked three taxa (diatoms, coccolithophorids, and dinoflagellates) from October 1948 to October 1949 at weather Station M (66° N, 2° E). The three taxa followed a similar phenology reaching concentrations of 1–10 thousands of organisms/liter in spring and less than 1 thousands of organisms/liter in winter. However, the species inventory was not exhaustive, (some species had not yet been discovered) and winter sampling likely reflected the lower thresholds in the detection method rather than actual values.

Alternatively we proceeded to quantify the division rate using the physiological model of Geider et al. (1997) together with the class-specific photo-physiological parameters estimated by Uitz (2006) for three major phytoplankton classes (micro-, nano-, and pico-phytoplankton). We will show that the model predicts very similar division rates for the three phytoplankton classes. Most importantly, the small difference in division rates will be shown to be much smaller than the overall increases in the averaged μ at bloom onset. Thus, uncertainty in overall species composition does not appear to contribute major uncertainty in the estimate of division rates.

Geider et al. (1997) proposed that the nutrient-saturated division rates are well described by the equation:

$$\mu(z,t) = \mu_{\max}\left(1 - \mathrm{e}^{-\frac{\alpha\ \mathrm{chl} \times \theta\mathrm{c}\ \times\ \mathrm{iPAR(z,t)}}{\mu_{\max}}}\right), \quad (9)$$

where $\mu_{\max}$ is the maximum value of the division rate under light-saturated conditions (s^{-1}), α_{chl} is the Chl *a*-specific initial slope of the photosynthesis-irradiance curve ($gC\,gChla^{-1}\,\mu mol^{-1}$ photons m^2), θ_c is the chlorophyll to carbon ratio. Here we are interested in sustained growth rates for at least a day, not transient growth rates lasting

BGD
12, 13631–13673, 2015

only a few hours. We will therefore average Eq. (9) over a full day (indicating by an overbar) in addition to integrating over the full ML depth:

$$\langle \bar{\mu} \rangle = \frac{1}{1\,\text{day}} \int_0^{1\,\text{day}} \int_0^{H} \mu_{\max} \left(1 - e^{-\frac{\alpha\text{chl} \times \theta\text{c} \times \text{iPAR(z,t)}}{\mu_{\max}}}\right) \text{d}z\,\text{d}t. \quad (10)$$

The vertical profile of iPAR (μmol photons $m^{-2}\,s^{-1}$) is modeled through:

$$\text{iPAR}(z,t) = \text{iPAR}(0,t)e^{K \times z} \quad (11)$$

where K (m^{-1}) is the diffuse attenuation coefficient for PAR. We ignore K variations throughout the day and within the euphotic layer. K is estimated from the euphotic layer depth following:

$$K = \log(0.01)/Z_{\text{eu}}. \quad (12)$$

The chlorophyll to carbon ratio was estimated using a float-derived empirical relationship between θ_c and the daily average surface PAR, $i\bar{\text{PAR}}(0)$, weighted for daylength (µmol photons $m^{-2}\,h^{-1}$) in the subpolar North Atlantic ($\sim 62^\circ$ N) (Xing et al., 2014):

$$\theta_c = 0.016 + (0.033 - 0.016) \times \exp\left(-3 \times \frac{\text{iPAR}(0)}{\text{d/}} \times \exp\left(-0.5 \times \text{K} \times \text{H}\right)\right). \quad (13)$$

The chlorophyll to carbon ratio was estimated to be the same for the three phytoplankton classes. This assumption is reasonable given that in the limit of low light, Eq. (13) reduces to $\theta_c = 0.033$ a typical value observed in phytoplankton cells acclimated to extremely low light (see Geider et al., 1997, Table 2).

The class-specific $\mu_{\max}$ and α_{chl} are taken from Table II-6 in Uitz[1] (2006) and are reported in Table 2.

[1] Uitz (2006) reported values for maximum chlorophyll-normalized primary production $P^B_{\max}$ (gC $gChla^{-1}\,h^{-1}$) and thus the class-specific $\mu_{\max}$ was determined by multiplying the class-specific $P^B_{\max}$ by θ_c.

BGD
12, 13631–13673, 2015

The time series of $\frac{1}{H}\langle\bar{\mu}\rangle$ for the three-phytoplankton classes are shown in Fig. 2e for the IMR2 sample float. The dramatic seasonal changes in $\frac{1}{H}\langle\bar{\mu}\rangle$ trump any small differences across the three classes. The same holds for all other float years. Given the small differences, we will report only the $\frac{1}{H}\langle\bar{\mu}\rangle$ values averaged among the three classes in the rest of the paper.

4.1.2 Phytoplankton loss rates

Phytoplankton loss rates are given by the sum of phytoplankton respiration rate, grazing, viral lysis and parasitism. These terms, and in particular the last three, are very difficult to estimate in situ. Instead we will estimate the loss rates as the residual between the division rates, $\langle\bar{\mu}\rangle$, and the phytoplankton accumulation rates averaged over a day.

Assuming that phytoplankton concentration and loss rates are uniform over the ML depth, we can derive two separate equations to estimate loss rates during time of ML deepening and shoaling, respectively (Behrenfeld, 2010). When the mixed layer deepens and entrains fluid with no phytoplankton from below, Eq. (4) can be time and vertically integrated to obtain an equation for the standing stock $\Pi = \int_{-H}^{0} P(z)\,\mathrm{d}z$,

$$\frac{\mathrm{d}\Pi}{\mathrm{d}t} = \frac{1}{H}\langle\bar{\mu}\rangle\Pi - \overline{m}\Pi, \tag{14a}$$

from which we can estimate the loss rates,

$$\overline{m} = \frac{1}{H}\langle\bar{\mu}\rangle - \frac{1}{\Pi}\frac{\mathrm{d}\Pi}{\mathrm{d}t}. \tag{14b}$$

During time when the ML shoals and leaves phytoplankton behind, the vertical average of Eq. (4) gives

$$\frac{\mathrm{d}P}{\mathrm{d}t} = \frac{1}{H}\langle\bar{\mu}\rangle P - \overline{m}P, \tag{15a}$$

BGD
12, 13631–13673, 2015

and

$$\overline{m} = \frac{1}{H}\langle\bar{\mu}\rangle - \frac{1}{P}\frac{\mathrm{d}P}{\mathrm{d}t}. \quad (15b)$$

Equations (14b) and (15b) are very similar except for the appearance of a standing stock Π versus a concentration P. In Sect. 5, we will estimate the phytoplankton loss rates from Eqs. (14a) or (15b) depending on whether the ML is deepening or shoaling and using our estimates of $\langle\bar{\mu}\rangle$ and the rates of float [Chl *a*] accumulation.

4.2 Critical photoperiod hypothesis

In the Nordic Seas, the insolation drops dramatically in winter. As one moves of the Arctic Circle, there are progressively longer periods of complete winter darkness, the polar nights. It is not clear that the critical depth framework is appropriate to study blooms under these conditions. The very concept of critical depth assumes that growth is always possible at the ocean surface, while this is not the case during polar nights. Under these conditions, the focus must shift on understanding how phytoplankton cells survive the winter darkness to give rise to a bloom in spring. With no energy to photosynthesize, cells will likely strive to reduce losses due to metabolic respiration, grazing pressure, parasitism, and viral infections. There is literature, reviewed below, suggesting that the cells enter in a dormant state during polar nights and wake up when the daylength crosses some threshold.

Eilertsen (1995) studied the onset of spring blooms in the coastal waters of the Nordic Seas. While coastal blooms may be different from open ocean blooms – the focus of our study – some key findings are worth reviewing. These blooms are dominated by marine diatoms in the early stages and begin approximately the same calendar day every year, despite highly variable year-to-year environmental conditions. Field studies showed that in the coastal waters of Northern Norway, the marine diatoms turn into resting spores during winter to drastically reduce respiration and survive several weeks of darkness (Degerlund and Eilertsen, 2010). The heavy spores sink to the bottom a

BGD
12, 13631–13673, 2015

few hundred meters below the surface into permanent darkness. However, they are occasionally re-suspended towards the surface by sudden mixing events triggered by atmospheric storms. Eilertsen et al. (1995) speculated that the spores germinate when the daylength exceeds a critical threshold; estimated between 7 and 12 h (Eilertsen and Wyatt, 2000). The "critical daylength hypothesis" differs fundamentally from "the critical depth hypothesis" in that the bloom onset is not associated with either mixing layer depth or biological losses. Note that this survival strategy is not specific to diatoms. Many species of dinoflagellates and chrysophytes produce cysts at the end of summer or in response to environmental stimuli, such as nutrient limitation, and remain dormant until the following spring. Some are known to germinate in response to light or nutrient stimulation. Others germinate after a specific period of time or in response to photoperiod (McMinn and Martin, 2013).

A daylength control has never been documented in the open ocean of the Nordic Seas, possibly due to the dearth of ocean color measurements in winter when cloud coverage is ubiquitous. Moreover, in the open ocean the hypothesis must be modified because the photoperiod can be shorter than the daylength, when strong mixing keeps cells below the euphotic layer for some part of the daytime as shown in Fig. 4. In the appendix, we derive an approximate formula to calculate the photoperiod in the open ocean as a function of daylength, euphotic layer depth and strength of mixing. In Sect. 5, we will use our estimate of the photoperiod to test whether the first accumulation of the season detected by the fluorometer occurred at a critical photoperiod, supporting the hypothesis that the onset of the Nordic Seas blooms is consistent with a critical photoperiod hypothesis.

5 Testing bloom onset hypotheses

Using the theoretical framework that we developed in the last section, we will now test the two bloom onset scenarios that emerged from the preliminary analysis of the float data.

BGD
12, 13631–13673, 2015

5.1 Critical depth hypothesis

First, we test whether the start of the Nordic Seas blooms is consistent with the critical depth hypothesis, i.e. the blooms begin when $\frac{1}{H}\langle\bar{\mu}\rangle \geq m$. To do so, $\langle\bar{\mu}\rangle$ is estimated according Eq. (10) using Antoine and Morel's (1996) model of PAR and the [Chl *a*]-based estimate of K. The phytoplankton loss rates are then computed as a residual between division and accumulation rates as described in the previous section. m was in the range of 0.0–0.4 day^{-1} with a median value of 0.06 day $^{-1}$. Loss rates could not be estimated prior to t_E, because measurements of [Chl *a*] are dominated by noise during Δt_{onset}. The median value across all eight years is used as representative of an upper bound on the winter phytoplankton loss rates; respiration and grazing are likely to progressively increase through Δt_{onset} as the Nordic Seas emerge out of the polar night. A loss rate of within a range of 0.05–0.1 day^{-1} is typically used to parametrize phytoplankton non-grazing mortality rate (eg., Behrenfeld et al., 2013; Dutkiewicz et al., 2015; Evans and Parslow, 1985; Moore et al., 2002), thus our estimate support the hypothesis that grazing was very weak in winter. In order to test if the bloom onset was consistent with the critical depth hypothesis we next test whether $\frac{1}{H}\langle\bar{\mu}\rangle$ exceeded 0.06 day^{-1} during Δt_{onset}.

Figure 5a shows the time series of $\frac{1}{H}\langle\bar{\mu}\rangle$ with time axis shifted so that for each of the eight years the origin is at t_E. In all years, $\frac{1}{H}\langle\bar{\mu}\rangle$ exceeded 0.06 day^{-1} within the month prior to $t = t_E$. Moreover, as anticipated in the preliminary data analysis, $\frac{1}{H}\langle\bar{\mu}\rangle$ primarily tracks the increase in insolation. Fig. 5b shows that the dramatic increase in $\frac{1}{H}\langle\bar{\mu}\rangle$ disappears if the seasonal increase in surface insolation is ignored – iPAR$(0,t)$ was replaced with a periodic repetition of the daily cycle of incoming surface insolation on 1 March at 70°. Surprisingly, even the deep MLs sampled by floats IMR2 and IMR3 had little impact in delaying the increase in division rates driven by the surface insolation. Indeed, it would be argued that the only reason for the delay in t_E for these two years is because the MLs were very deep and the [Chl *a*] remained too diluted to be detected by the fluorometer.

BGD
12, 13631–13673, 2015

In conclusion, our data are consistent with the hypothesis that the Nordic Seas blooms start according to the critical depth hypothesis. But the analysis falls short of proving that the deepening of critical depth at the end of winter is the trigger of the bloom. Such a proof would require accurate estimates of winter division and loss rates, which are simply impossible to obtain with present technology. Moreover, fluorometers with lower noise threshold are needed to document the first accumulation of chlorophyll in the Nordic Seas winter, when concentrations are extremely low.

5.2 Critical photoperiod hypothesis

Next, we test whether the start of the Nordic Seas blooms is consistent with the critical photoperiod hypothesis. To do so, we estimate the photoperiod at the time when the fluorometers detected the first accumulation of biomass, i.e., at $t = t_E$. The photoperiod is calculated with the algorithm presented in the appendix. Notice that in this section we therefore assume that the bloom onset coincided with the first increase detected in fluorescence.

In Sect. 3, we anticipated that at $t = t_E$, the daylength was between 9 and 11 h for the six years when biomass accumulation was detected with mixed layers shallower than 200 m. The formula we developed in the appendix suggests that for these six blooms the daylength is a pretty accurate estimate of the photoperiod, because the cells remained in the euphotic layer for the whole daylength when the surface heat losses are smaller than 200 W m^{-2}. The onset of these blooms is therefore consistent with a critical photoperiod of 10 ± 1 h. The daylength increases by one hour every 10 days along the Arctic circle, so the photoperiod cannot be determined to better than one hour with the 10-day float sampling frequency.

In the remaining two blooms with winter mixed layers much deeper than 200 m, the fluorometers detected the first biomass accumulation when the heat losses and hence mixing subsided at the end of winter. In the weeks preceding $t = t_E$, when the daylength was between 9 and 14 h, the heat losses were constantly above 200 W m^{-2} (Fig. 3a). In the appendix, we show that the strong heat losses generated such intense mixing that

BGD
12, 13631–13673, 2015

the cells never experienced more than 8 h of light. Hence, the photoperiod experienced by the cells did not reach the 10 h threshold until the cooling finally subsided at the end of March. Therefore, the onset of these two late blooms is also consistent with a critical photoperiod of 10 ± 1 h.

To summarize, the bloom onset is consistent with the photoperiod hypothesis if the chlorophyll started to accumulate when it was first detected by the fluorometer. However, it is also possible that the bloom started earlier according to the critical depth hypothesis, if some weak accumulation started earlier in the season at levels too low to be detected by fluorometers. Our opinion is that the photoperiod hypothesis is more likely to be correct, because it is hard to believe that the co-occurrence of a critical photoperiod of 10 ± 1 h and the increase in chlorophyll detected by the fluorometers is mere coincidence.

6 Conclusions

In the Nordic Seas, north of the Arctic Circle, insolation drops so dramatically in winter that phytoplankton growth is impossible for days to weeks during polar nights. The goal of this paper was to investigate how do phytoplankton populations survive such harsh winter conditions and what triggers their resurgence in spring. Satellite data are hardly ever available at these latitudes due to continuous cloud coverage. Instead, we used in-situ data of [Chl *a*] and CTD from five bio-optical floats deployed in this region.

Not surprisingly, the Chl *a* concentrations dropped dramatically in winter, during polar nights, to values lower than reported by floats south of the Arctic Circle. The values were so low that they were below or at the noise threshold levels of the traditional fluorometers mounted on the floats. After a few months, at the end of winter, the Chl *a* concentrations started increasingly very rapidly. We cannot definitively conclude that this increase marked the bloom onset, because low Chl *a* accumulation could have started earlier in the season at levels below the fluorometers detection levels. This uncertainty in the exact timing of the bloom onset implies that the float data are consis-

BGD
12, 13631–13673, 2015

tent with two possible scenarios for the onset of blooms in the Nordic Seas: the critical depth hypothesis and the critical photoperiod hypothesis.

According to the critical depth hypothesis, blooms start when phytoplankton division rates exceed their loss rates. The float data suggest that changes in the ML depth and heat losses had little impact on the division rates in the Nordic Seas at the end of winter. Furthermore, the winter grazing rates were lower than non-grazing mortality due to respiration, parasitism and viral lysis. Thus dilution of grazers did not appear to have much an effect on the increase in phytoplankton populations. Insolation instead increased very rapidly at the end of winter north of the Arctic Circle and may have driven an increase in division rates large enough to overcome losses. According to our analysis the increased insolation ought to have triggered the blooms before they were detected by the fluorometers. A possible scenario, given that the fluorometer signals were dominated by noise in winter. But a scenario we cannot test with our data.

A second more tantalizing scenario is also consistent with the data. In all years sampled by the floats, the increase in Chl *a* concentrations was detected when the phytoplankton experienced a photoperiod of ten hours, i.e. when phytoplankton experienced ten light hours in a day for the first time in the season. The critical photoperiod was equal to a 10 h daylength, when mixing was weak, but it corresponded to a longer daylength, when mixing was strong and kept cells away from the well-lit surface. We speculate that similarly to what has been documented in the coastal waters of the Nordic Seas, phytoplankton enters in resting stages during polar night in order to minimize energy expenditure. Unlike in coastal waters, the resting stage cannot be in the form of spores of cysts that are too dense to float in the open ocean. Rather the resting stage must be in the form of vegetative cells whose density is closer to that of the water and can remain re-suspended for long periods of time (D'Asaro, 2008.) We tend to favor this second explanation, because it is hard to believe that the co-occurrence of the bloom onset with a specific photoperiod is pure coincidence. However future work will have to investigate how phytoplankton cells survive through polar nights to assess whether the photoperiod hypothesis is tenable.

BGD
12, 13631–13673, 2015

Theory and models of high latitude ocean blooms do not consider the possibility that phytoplankton enter and exit from resting stages in response to changes in photoperiod. This omission can potentially impact the whole representation of these ecosystems, because the timing of bloom initiation has been shown to impact on all the trophic levels affecting, for example, the survival of larval fish (Platt et al., 2003) and the hatching time of shrimp eggs (Koeller et al., 2009). Furthermore, an accurate representation of the timing and evolution of the bloom is crucial to represent the ocean ecosystem response to climate change and its impact on the ocean carbon budget.

Appendix A: Calculation of the photoperiod

The photoperiod is the time spent by a cell in the euphotic layer within one day. In the open ocean this time depends on the length of daytime, the thickness of the euphotic layer and the trajectories of a cell in the turbulent mixed layer. The estimation of the euphotic layer depth and the calculation of the cell trajectories are discussed below.

A1 Calculation of the euphotic layer depth

The euphotic layer depth (Z_{eu}), defined as the depth at which the light intensity is 1 % of its surface value, was calculated from the float $[Chl]_{ML}$ using the empirical relationship derived by (Morel et al., 2007) from a global datasets of ship-based measurements of Z_{eu} and surface [Chl *a*] (Morel et al., 2007) :

$$\log_{10}Z_{eu} = 1.524 - 0.436 \times \log_{10}[Chl]_{ML} - 0.0145 \times (\log_{10}[Chl]_{ML})^2 + 0.0186 \times (\log_{10}[Chl]_{ML})^3 \quad \text{(A1)}$$

In winter, when the ML [Chl *a*] was too low to be detected by the fluorometer, the euphotic layer depths estimated by Eq. (A1) was in the range of 150 to 170 m with a mean value of 165 ± 5 m. In the following calculations, the mean value across all eight years are used as representative of a lower bound on the winter euphotic layer depth.

BGD
12, 13631–13673, 2015

A2 Calculation of the turbulent velocity in a convective mixed layer

Mixed layer turbulence can be driven by heat fluxes, freshwater fluxes or winds. In the North Atlantic, upper ocean turbulence is generated by the surface heat with minor contributions from freshwater fluxes and winds (Ferrari et al., 2014). Hence the analysis will focus on mixed layers forced by heat fluxes.

The root mean square vertical velocity in a mixed layer forced by thermal convection in a nonrotating environment follows the following scaling verified by numerous laboratory experiments (Deardorff and Willis, 1985; Fernando et al., 1991), and numerical simulations (Deardorf, 1972; Molemaker and Dijkstra, 1997),

$$w_{\mathrm{rms}} = A|B_0 H|^{1/3}, \tag{A2}$$

where H is the mixing layer depth, i.e the depth to which mixing penetrates (or equivalently the mixed layer depth, since mixing typically extends to the whole mixed layer during winter convection). B_0 is the surface buoyancy flux, and A is an order one coefficient of proportionality. When the surface density is only affected by temperatures changes, B_0 can be related to the surface heat flux $B_0 = \alpha g Q_0 / (c_P \rho_0)$, where c_{P} is the heat capacity, α is the thermal expansion coefficient, ρ_0 is the water density, and g is the gravitational acceleration.

D'Asaro and collaborators (Asaro, 2001, 2008; Steffen and Asaro, 2002; Tseng and Asaro, 2004) using trajectories of Lagrangian floats have shown that the scaling applies also to winter convection in the real ocean. In particular Steffen and D'Asaro (2002) found that Eq. (A2) applies to convection in the North Atlantic with a coefficient A in the range 0.3–0.6. In the following calculations we will set $A = 0.45 \pm 0.15$.

A3 Calculation of the cell residence time in the euphotic layer during a convection event

Armed with estimates of the euphotic layer depth and the magnitude of the turbulent velocity, we can now estimate the fraction of time that a particle spends in the euphotic

BGD
12, 13631–13673, 2015

layer during convection. We idealize the looping trajectories in turbulent convective cells as periodic oscillations between the ocean surface and the mixing layer depth H,

$$z(t) = H/2[\cos(\Omega t) - 1], \tag{A3}$$

where $T = 2\pi/\Omega$ is the period of the oscillations. The vertical velocity of the particles is therefore given by

$$w = \mathrm{d}z/\mathrm{d}t = -H\Omega/2\sin(\Omega t). \tag{A4}$$

Averaging w^2 over a period, we obtain the root-mean-square velocity, $w_{\mathrm{rms}} = \sqrt{2}/2H\Omega$. This expression, together with the scaling law for w_{rms}, in Eq. (A2), gives a scaling law for the frequency Ω and the period of the oscillations in the mixed layer,

$$\Omega = 2\sqrt{2A}|B_0 H|^{1/3}/H, \text{ and } T = \pi/\sqrt{2H/A}|B_0 H|^{1/3} \tag{A5}$$

To assess the skill of the scaling for T, we compared the prediction of T form Eq. (A5) with two estimates of the overturning timescale from Lagrangian floats deployed in the North Atlantic (Steffen and Asaro, 2002). The results are reported in Table C1. Equation (A5) predicts overturning timescales of 1.5 ± 0.6 and 1.3 ± 0.5 days using the observed mixed layer depths and heat fluxes in good agreement with float based estimates of 1.2 and 1.6 days respectively.

The residency time of particles in the euphotic layer is now easily computed as the time a trajectory spends between the surface and the euphotic layer depth Z_{eu}. Assuming that the overturning timescale T is longer than the length of daytime, then the particles will visit the euphotic layer only once per day for a period of time given by,

$$T_{\mathrm{eu}} = H/\sqrt{2A^{-1}}|B_0 H|^{-1/3}\,\mathrm{acos}\,(1 - 2Z_{\mathrm{eu}}/H). \tag{A6}$$

Figure B1 plots the residency time T_{eu} as a function of mixed layer depth and heat flux, for the typical euphotic depth during winter in the region considered, $Z_{\mathrm{eu}} = 165$ m. For

BGD
12, 13631–13673, 2015

MLDs close to the euphotic depth, the particle speed are slow enough that cells in the euphotic layer experience light most of the daytime. For MLDs deeper than 200 m, the time spent in the euphotic layer decreases with increasing heat flux and is very weakly dependent on the mixing layer depth. One can understand this dependence taking the limit of Eq. (A6) for $Z_{eu}/H << 1$,

$$T_{eu}\ 2/A\sqrt{2}Z_{eu}^{1/2}H^{1/6}|B_0|^{-1/3}. \quad \text{(A7)}$$

The increase in w_{rms} for increasing H is offset by the decrease in speed close to the surface resulting into a weak dependence on H.

The residency time of phytoplankton cells in the upper 165 m at the onset of all 8 blooms is shown in Fig. B1. The surface heat flux was estimated as the median value of Q_0 in the time interval between the last profile before t_E and the profile at t_E. Its uncertainty was defined as the semi-interquartile range of Q_0 in the same time interval. For most blooms H was estimated as the median ML depth between the last profile before t_E and the profile at t_E. The uncertainty in H was set equal to the difference in ML depth between the last profile before t_E and the profile at t_E. For the blooms IMR3 2010–2011 and IMR3 2011–2012, the [Chl *a*] was observed to increase in a layer shallower than the density-based estimate of the ML depth. The ML depth is a poor estimator of the mixing layer depth as it may miss any slight restratification near the surface and it may also record past deeper mixing events. For these two blooms, it is therefore more appropriate to estimate H as the depth of the layer where we observed an increase of [Chl *a*], which likely tracks the region where mixing is active.

Figure B1 shows that H was shallower than Z_{eu} at t_E of five of the blooms and therefore the cells remained in the euphotic layer for the whole length of daytime. At t_E of the remaining three, the cell residency time in the upper 165 m is estimated to have been longer than or equal to 10 h.

BGD
12, 13631–13673, 2015

A4 Calculation of the photoperiod

The photoperiod is the number of hours for which phytoplankton cells are exposed to light during the day, i.e, the daily time spent in the euphotic layer. If the residency time T_{eu} is longer than the daylength or the mixing layer is shallower than the euphotic depth, then the photoperiod for cells in the euphotic layer is equal to the daylength; otherwise the photoperiod is shorter and equal to T_{eu}. The Table C2 summarizes the daylength, H, Q_0 and our estimate of T_{eu} at each bloom onset.

In six blooms, t_E occured when the daylength was between 9 and 11 h (Table C2). During that period, the surface heat losses remained smaller than 200 W m^{-2}. For heat fluxes of this magnitude, cells spent more than 9 h in the upper 165 m as per Fig. B1, while the daylength was shorter. Hence the photoperiod was equal to the daylength and was between 9 and 11 h on the day of t_E. The two hour spread in photoperiod values most likely stems from the 10 day sampling of the floats, which is equivalent to a one hour change in daylength at the latitudes sampled by the floats. We conclude that the critical photoperiod when phytoplankton cells germinate is 9 h with an uncertainty of one hour for these six bloom events.

In the remaining two float years, t_E occurred when the daylength was around 14 h (Table C2). The two floats were within 30 km of each other at bloom onset, so the two events are not really independent. In both cases, the heat losses were constantly above 200 W m^{-2} as the daylength increased from 9 to 14 h, as can be seen in Fig. 3a looking at the 40 days prior to bloom onset. According to Fig. B1, such a strong heat flux generated enough mixing to prevent cells from experiencing more than 8 h of light. Thus, from the point of view of the cells, the photoperiod did not exceed 10 h until the surface heat fluxes decreased at the end of March and the daylength was already 14 h. We conclude that the bloom onset is consistent with a 10 h critical photoperiod for these two blooms as well.

The Supplement related to this article is available online at doi:10.5194/bgd-12-13631-2015-supplement.

BGD
12, 13631–13673, 2015

Acknowledgements. This paper represents a contribution to the E-AIMS projects, which is funded by the European Research Council (grant agreement no. 312642). Alexandre Mignot and Raffaele Ferrari acknowledge NSF support through award OCE-1155205. We thank the crew of the various cruises who deployed the Bio-optical floats used in the present study. We also acknowledge many insightful conversations with Herve Claustre, Glenn Flierl and Emmanuel Boss.

References

Antoine, D. and Morel, A.: Oceanic primary production: 1. Adaptation of a spectral light-photosynthesis model in view of application to satellite chlorophyll observations, Glob. Biogeochem. Cy., 10, 43–55, 1996.

Behrenfeld, M. J.: Abandoning Sverdrup's Critical Depth Hypothesis on phytoplankton blooms, Ecology, 91, 977–989, 2010.

Behrenfeld, M. J., Doney, S. C., Lima, I., Boss, E. S., and Siegel, D. A.: Annual cycles of ecological disturbance and recovery underlying the subarctic Atlantic spring plankton bloom, Glob. Biogeochem. Cy., 27, 526–540, 2013.

Boss, E., Swift, D., Taylor, L., Brickley, P., Zaneveld, R., Riser, S., Perry, M. J., and Strutton, P. G.: Observations of pigment and particle distributions in the western North Atlantic from an autonomous float and ocean color satellite, Limnol. Oceanogr., 53, 2112–2122, 2008.

Brainerd, K. and Gregg, M.: Surface Mixed and Mixing Layer Depths, Deep-Sea Res. Pt. I, 42, 1521–1543, 1995.

D'Asaro, E. A.: Turbulent vertical kinetic energy in the ocean mixed layer, J. Phys. Oceanogr., 31, 3530–3537, 2001.

D'Asaro, E. A.: Convection and the seeding of the North Atlantic bloom, J. Mar. Syst., 69, 233–237, 2008.

Deardorf, J.: Numerical Investigation of Neutral and Unstable Planetary Boundary-Layers, J. Atmospheric Sci., 29, 91–115, 1972.

Deardorff, J. and Willis, G.: Further Results from a Laboratory Model of the Convective Planetary Boundary-Layer, Bound.-Layer Meteorol., 32, 205–236, 1985.

Dee, D. P., Uppala, S. M., Simmons, A. J., Berrisford, P., Poli, P., Kobayashi, S., Andrae, U., Balmaseda, M. A., Balsamo, G., Bauer, P., Bechtold, P., Beljaars, A. C. M., van de Berg, L.,

BGD
12, 13631–13673, 2015

Bidlot, J., Bormann, N., Delsol, C., Dragani, R., Fuentes, M., Geer, A. J., Haimberger, L., Healy, S. B., Hersbach, H., Holm, E. V., Isaksen, L., Kallberg, P., Koehler, M., Matricardi, M., McNally, A. P., Monge-Sanz, B. M., Morcrette, J.-J., Park, B.-K., Peubey, C., de Rosnay, P., Tavolato, C., Thepaut, J.-N., and Vitart, F.: The ERA-Interim reanalysis: configuration and performance of the data assimilation system, Q. J. R. Meteorol. Soc., 137, 553–597, 2011.

Degerlund, M. and Eilertsen, H. C.: Main Species Characteristics of Phytoplankton Spring Blooms in NE Atlantic and Arctic Waters (68–80° N), Estuar. Coast., 33, 242–269, 2010.

Dutkiewicz, S., Hickman, A. E., Jahn, O., Gregg, W. W., Mouw, C. B., and Follows, M. J.: Capturing optically important constituents and properties in a marine biogeochemical and ecosystem model, Biogeosciences, 12, 4447–4481, doi:10.5194/bg-12-4447-2015, 2015.

Eilertsen, H. and Wyatt, T.: Phytoplankton models and life history strategies, South Afr. J. Mar. Sci., 22, 323–338, 2000.

Eilertsen, H., Sandberg, S., and Tollefsen, H.: Photoperiodic Control of Diatom Spore Growth – a Theory to Explain the Onset of Phytoplankton Blooms, Mar. Ecol. Prog. Ser., 116, 303–307, 1995.

Evans, G. T. and Parslow, J. S.: A Model of Annual Plankton Cycles, Biol. Oceanogr., 3, 327–347, 1985.

Fernando, H., Chen, R., and Boyer, D.: Effects of Rotation on Convective Turbulence, J. Fluid Mech., 228, 513–547, 1991.

Ferrari, R., Merrifield, S. T., and Taylor, J. R.: Shutdown of convection triggers increase of surface chlorophyll, J. Mar. Syst., 147, 116–122, doi:10.1016/j.jmarsys.2014.02.009, 2014.

Forsythe, W., Rykiel, E., Stahl, R., Wu, H., and Schoolfield, R.: A Model Comparison for Daylength as a Function of Latitude and Day of Year, Ecol. Model., 80, 87–95, 1995.

Geider, R. J., MacIntyre, H. L., and Kana, T. M.: Dynamic model of phytoplankton growth and acclimation: Responses of the balanced growth rate and the chlorophyll a:carbon ratio to light, nutrient-limitation and temperature, Mar. Ecol. Prog. Ser., 148, 187–200, 1997.

Gran, H. H. and Braarud, T.: A Quantitative Study of the Phytoplankton in the Bay of Fundy and the Gulf of Maine (including Observations on Hydrography, Chemistry and Turbidity), J. Biol. Board Can., 1, 279–467, 1935.

Gregg, W. and Carder, K.: A Simple Spectral Solar Irradiance Model for Cloudless Maritime Atmospheres, Limnol. Oceanogr., 35, 1657–1675, 1990.

BGD
12, 13631–13673, 2015

Halldal, P.: Phytoplankton investigations from weather ship M in the Norwegian Sea, 1948–1949, Including observations during the “Armauer Hansen” cruise, July, 1949, I kommisjon hos J. Dybwad, Oslo, 1953.
Kara, A. B., Rochford, P. A., and Hurlburt, H. E.: An optimal definition for ocean mixed layer depth, J. Geophys. Res.-Oceans, 105, 16803–16821, 2000.
Kara, A. B., Rochford, P. A., and Hurlburt, H. E.: Mixed layer depth variability over the global ocean, J. Geophys. Res.-Oceans, 108, C3, doi:10.1029/2000JC000736, 2003.
Koeller, P., Fuentes-Yaco, C., Platt, T., Sathyendranath, S., Richards, A., Ouellet, P., Orr, D., Skuladottir, U., Wieland, K., Savard, L., and Aschan, M.: Basin-Scale Coherence in Phenology of Shrimps and Phytoplankton in the North Atlantic Ocean, Science, 324, 791–793, 2009.
McMinn, A. and Martin, A.: Dark survival in a warming world, Proc. Biol. Sci., 280, 20122909, doi:10.1098/rspb.2012.2909, 2013.
Molemaker, M. J. and Dijkstra, H. A.: The formation and evolution of a diffusive interface, J. Fluid Mech., 331, 199–229, 1997.
Moore, J. K., Doney, S. C., Kleypas, J. A., Glover, D. M., and Fung, I. Y.: An intermediate complexity marine ecosystem model for the global domain, Deep-Sea Res. Pt. I, 49, 403–462, 2002.
Morel, A., Huot, Y., Gentili, B., Werdell, P. J., Hooker, S. B., and Franz, B. A.: Examining the consistency of products derived from various ocean color sensors in open ocean (Case 1) waters in the perspective of a multi-sensor approach, Remote Sens. Environ., 111, 69–88, 2007.
Platt, T., Fuentes-Yaco, C., and Frank, K. T.: Spring algal bloom and larval fish survival, Nature, 423, 398–399, 2003.
R Development Core Team: A language and environment for statistical computing, R Foundation for Statistical Computing, Vienna, Austria, ISBN 3-900051-07-0, available at: http://www.R-project.org, 2013.
Riley, G.: Factors Controlling Phytoplankton Populations on Georges Bank, J. Mar. Res., 6, 54–73, 1946.
Skjelvan, I., Olsen, A., Anderson, L. G., Bellerby, R. G. J., Falck, E., Kasajima, Y., Kivimäe, C., Omar, A., Rey, F., Olsson, K. A., Johannessen, T., and Heinze, C.: A review of the inorganic carbon cycle of the Nordic Seas and Barents Sea, in: Geophysical Monograph Series, vol. 158, edited by: Drange, H., Dokken, T., Furevik, T., Gerdes, R., and Berger, W., Amer-

BGD
12, 13631–13673, 2015

ican Geophysical Union, Washington, DC, available at: http://www.agu.org/books/gm/v158/158GM11/158GM11.shtml (last access: 25 April 2014), 157–175, 2005.
Steffen, E. L. and D'Asaro, E. A.: Deep convection in the Labrador Sea as observed by Lagrangian floats, J. Phys. Oceanogr., 32, 475–492, 2002.
Sverdrup, H. U.: On Conditions for the Vernal Blooming of Phytoplankton, J. Cons., 18, 287–295, 1953.
Takahashi, T., Sutherland, S. C., Sweeney, C., Poisson, A., Metzl, N., Tilbrook, B., Bates, N., Wanninkhof, R., Feely, R. A., Sabine, C., Olafsson, J., and Nojiri, Y.: Global sea-air CO_2 flux based on climatological surface ocean pCO_2, and seasonal biological and temperature effects, Deep-Sea Res. Pt. I, 49, 1601–1622, 2002.
Taylor, J. R. and Ferrari, R.: Shutdown of turbulent convection as a new criterion for the onset of spring phytoplankton blooms, Limnol. Oceanogr., 56, 2293–2307, 2011.
Tseng, R. S. and D'Asaro, E. A.: Measurements of turbulent vertical kinetic energy in the ocean mixed layer from Lagrangian floats, J. Phys. Oceanogr., 34, 1984–1990, 2004.
Uitz, J.: Structure des communautés phytoplanctoniques et propriétés photophysiologiques dans l'océan ouvert: Paramétrisation en vue d'applications à la couleur de l'océan., 2006.
Wong, A., Keeley, R., Carval, T., and the Argo Data Management Team: Argo quality control manual. Technical report, Argo Data Management team, 2010.
Xing, X., Claustre, H., Uitz, J., Mignot, A., Poteau, A., and Wang, H.: Seasonal variations of bio-optical properties and their interrelationships observed by Bio-Argo floats in the subpolar North Atlantic, J. Geophys. Res.-Oceans, 119, 7372–7388, 2014.

BGD
12, 13631–13673, 2015

Table 1. Relevant Information concerning the 6 bio-optical profiling floats used in this study.

Float	wmo number	Deployment location	Deployment date	Sensor failure date
IMR1	6900796	0.26° W, 67.68° N	30 May 2010	Optical sensors: 31 Oct 2012 CTD: 19 Jan 2013
IMR2	6900798	2.34° E, 69.09° N	02 Jul 2010	Optical sensors: 01 Nov 2012 CTD is still operational
IMR3	6900799	6.01° E, 70.03° N	06 Nov 2010	Optical sensors: 31 Oct 2012 CTD: 20 Sept 2013
IMR4	6902547	7.49 ° E,69.31° N	22 Jan 2014	ongoing
IMR5	6902544	0.05° E, 64.66° N	16 Nov 2013	ongoing
IMR6	6902545	7.54° E, 69.28° N	22 Jan 2014	ongoing

BGD
12, 13631–13673, 2015

Table 2. Photophysiological variables [μ_{max} (s^{-1}) α_{chl} (gC $gChla^{-1}$ μmol^{-1} photons m^2)] for the three phytoplankton classes.

	μ_{max} (s^{-1})	α_{chl} (gC $gChla^{-1}$ μmol^{-1} photons m^2)
Micro-phytoplankton	$11.80 \times 10^{-4} \times \theta_c$	7.78×10^{-6}
Nano-phytoplankton	$5.94 \times 10^{-4} \times \theta_c$	15.86×10^{-6}
Pico-phytoplankton	$5.42 \times 10^{-4} \times \theta_c$	7.50×10^{-6}

BGD
12, 13631–13673, 2015

Table C1. Surface heat flux Q_0, mixing layer depth H, and observed overturning time T_{obs} as reported in (Steffen and Asaro, 2002). The corresponding predicted overturning time T_{mod} is based on Eq. (A5) with the following parameters: $A = 0.45 \pm 15$, $c_P = 3986\,J\,Kg^{-1}\,°C$, $\alpha = 8.72 \times 10^{-4}\,°C^{-1}$, $g = 9.81\,m^2\,s^{-1}$, and $\rho_0 = 1027.764\,kg\,m^{-3}$ derived from the observed salinity and potential temperature at the sea surface in (Steffen and Asaro, 2002). The T_{mod} uncertainties ($\Delta\ T_{mod}$) are calculated as: $\Delta\ T_{mod}\,/\,T_{mod} = ((\Delta A/A) + (1/3)\ (\Delta H/H) + (1/3)\ (\Delta\ Q_0/Q_0))$, with ΔA, ΔH, and $\Delta\ Q_0$ being the uncertainties of A, H, and Q_0.

	1997	1998
Q_0 ($W\,m^{-2}$)	270 ± 40	150 ± 30
H (m)	960 ± 30	620 ± 20
T_{obs} (days)	1.2	1.6
T_{mod} (days)	1.5 ± 0.6	1.3 ± 0.5

BGD
12, 13631–13673, 2015

Table C2. Daylength (hours), mixing layer depth (H), surface heat flux Q_0 ($W\,m^{-2}$), the euphotic layer residency time (T_{eu}) and photoperiod at t_E. The daylength is the estimated value at t_E. The estimates for Q_0, H, and their uncertainty are discussed in the text. The estimates of T_{eu}, based on Eq. (A6), are only indicated if $H > Z_{eu} = 165$ m.

Bloom	Daylength (h)	H (m)	Q_0 ($W\,m^{-2}$)	T_{eu} (h)	Photoperiod (h)
IMR1 2010–2011	10	236 ± 60	−65 ± 70	12	10
IMR1 2011–2012	10	156 ± 30	−130 ± 60		10
IMR2 2010–2011	14	136 ± 120	−100 ± 100		14
IMR2 2011–2012	11	130 ± 15	−130 ± 20		11
IMR3 2010–2011	14	363 ± 313	−130 ± 120	10	10
IMR3 2011–2012	11	103 ± 7	−120 ± 20		11
IMR4 2013–2014	9	35 ± 20	−130 ± 40		9
IMR6 2013–2014	10	182 ± 10	−100 ± 40	11	10

BGD
12, 13631–13673, 2015

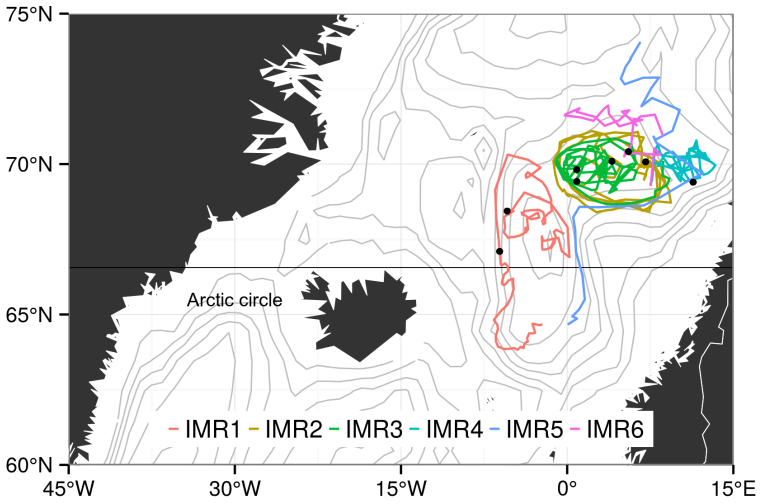

Figure 1. Trajectory of the floats used in the study. The black symbols show the location of the floats deployed North of the Arctic Circle (i.e., IMR1, IMR2, IMR3, IMR4 and IMR6) at t_E.

BGD
12, 13631–13673, 2015

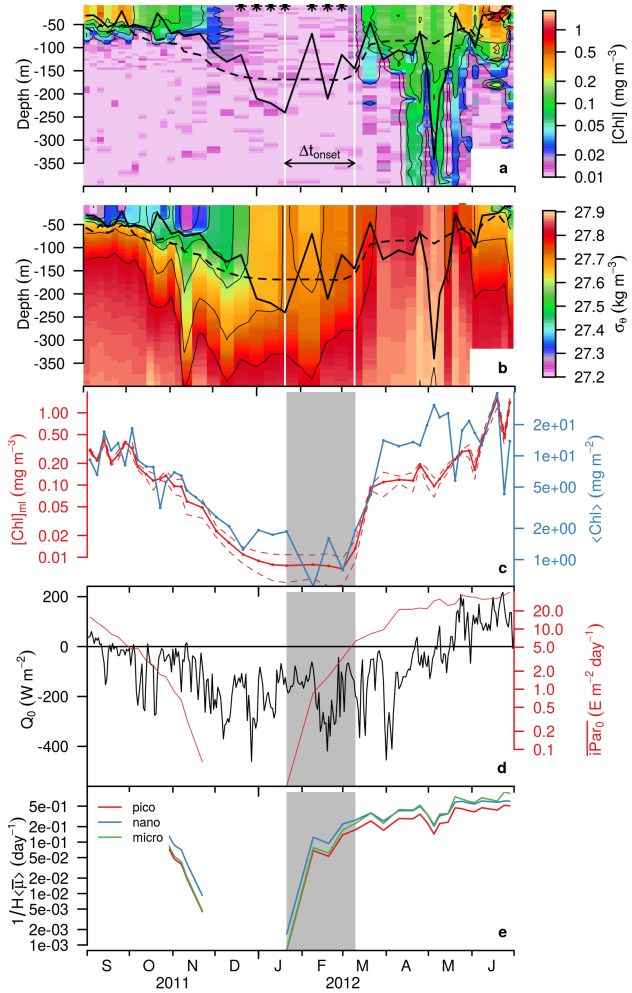

BGD
12, 13631–13673, 2015

Spring bloom onset in the Nordic Seas

A. Mignot et al.

Figure 2. Bloom observed by float IMR2 during the fall-spring 2011–2012. **(a)** Time evolution of the vertical distribution of [Chl *a*]; values lower than 0.01 mg m^{-3} have been set to 0.01 mg m^{-3}. The asterisks symbolize the vertical profiles where the ML fluorescence values are not significantly different from the deep fluorescence values. **(b)** Time evolution of the vertical distribution of potential density σ_θ. The continuous and dashed black lines are the mixed layer and euphotic layer depths, respectively. **(c)** Time series of the vertical integral and the average concentration of [Chl *a*] in the ML ($<$ Chl $>$, blue lines and $[\mathrm{Chl}]_{\mathrm{ML}}$, red line).The dashed lines are the standard deviations around the average cycle of $[\mathrm{Chl}]_{\mathrm{ML}}$. **(d)** Time series of the daily surface heat flux Q_0 (black line) and the daily average surface PAR corrected for cloud cover, $\overline{\mathrm{iPAR}}(0)$ (red line). **(e)** Time series of the class specific division rate (red: pico-, blue: nano-, green: microphytoplankton). The two white vertical lines and the gray shading indicate $\Delta t_{\mathrm{onset}}$; period of time during which bloom onset is possible. The second white vertical line indicates the sampling profile during which the ML fluorescence become significantly different from the deep fluorescence values (i.e., emergence from signal to noise, t_{E}).

BGD
12, 13631–13673, 2015

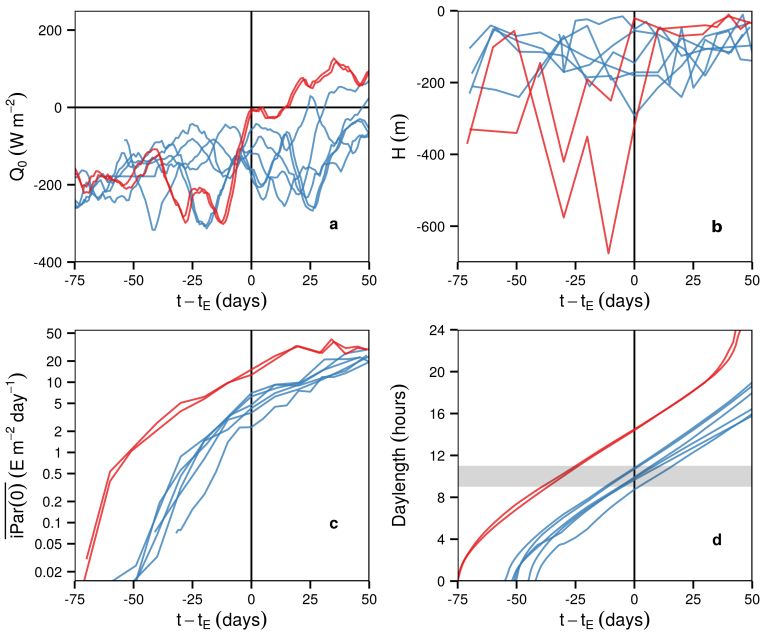

Figure 3. (a) Time series of surface heat flux (Q_0), **(b)** mixed layer depth (H), **(c)** the daily average surface PAR corrected for cloud cover ($\overline{\text{iPAR}}(0)$, and **(d)** daylength relative to the time of "emergence from signal to noise" t_E for the eight bloom events observed by the floats. The blue lines represent the cases where the first accumulation of biomass was associated with negative sea surface heat fluxes. The red lines represent the cases where the first accumulation of biomass associated with the shutdown of the wintertime cooling. A 10 day moving average has been applied to Q_0.

BGD
12, 13631–13673, 2015

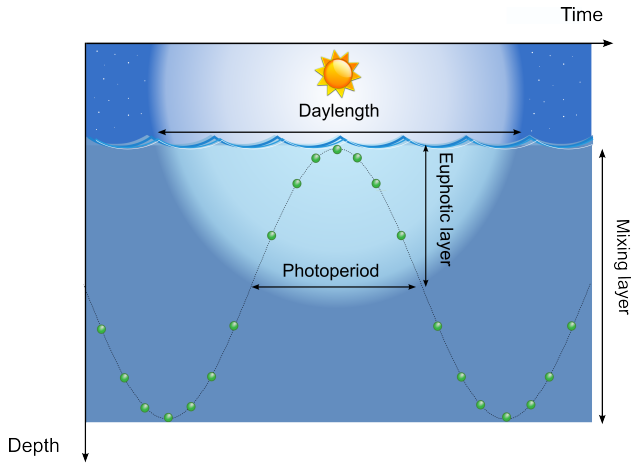

Figure 4. Schematic of the trajectory of a phytoplankton cells in the mixing layer. The photoperiod is the time spent by the cell in the euphotic layer. In the open ocean, this time depends on the daylength, the depth of the euphotic layer, the strength and the vertical extent of the turbulence mixing the cells.

BGD
12, 13631–13673, 2015

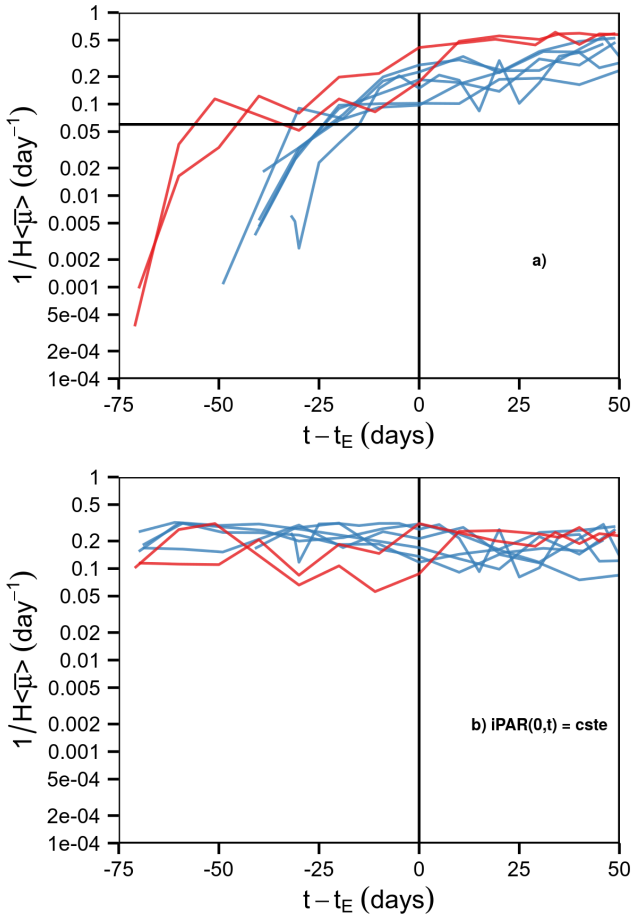

BGD
12, 13631–13673, 2015

Spring bloom onset in the Nordic Seas

A. Mignot et al.

Figure 5. Time series of the daily mixed layer-averaged and class-specific phytoplankton division rate averaged among the three phytoplankton classes ($1/H\langle\bar{\mu}\rangle$) based on Eq. (9) relative to $t = t_E$ for the eight events observed by the floats. The blue lines represent an accumulation of biomass associated with negative sea surface heat fluxes. The red lines represent accumulation of biomass associated with the shutdown of the wintertime cooling. The vertical black line represents the winter phytoplankton loss rates. **(a)** Estimates based a clear sky model of incoming irradiance for the days and latitudes sampled by each float ((Gregg and Carder, 1990). **(b)** Estimates based on the periodic repetition of the incoming irradiance on 1 March at 70° N.

BGD
12, 13631–13673, 2015

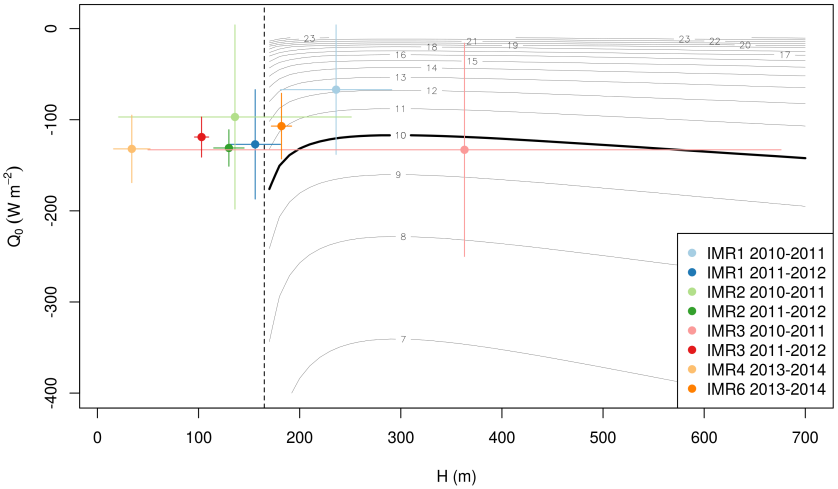

Figure B1. Residency time in the euphotic layer (T_{eu}) as a function of the mixing layer depth (H) and the surface heat flux (Q_0) at the onset time of the bloom. The estimates are based on Eq. (A6) with the following parameter values: $A = 0.45$, $c_P = 3984\,J\,Kg^{-1}\,°C$, $\alpha = 1.22 \times 10^{-4}\,°C^{-1}$, $g = 9.81\,m^2\,s^{-1}$, $\rho_{0=}1028\,kg\,m^{-3}$, ($c_P$, α and ρ_0 are the average values at the ten bloom onsets). The vertical dashed line is the euphotic depth, $Z_{eu} = 165\,m$. The estimates for Q_0, H and their uncertainty are discussed in the text.

BGD
12, 13631–13673, 2015